JPhys Materials

PAPER • OPEN ACCESS

Insights about the effect of metal–organic framework hybridization with graphene-like materials

To cite this article: Valentina Gargiulo *et al* 2024 *J. Phys. Mater.* **7** 045003

Journal of Physics: Materials

PAPER

Insights about the effect of metal–organic framework hybridization with graphene-like materials

Valentina Gargiulo[1], **Roberto Di Capua**[2,5,*], **Michael Vorochta**[3], **Giuliana Aquilanti**[4], **Tomáš Skála**[3], **Claudio Clemente**[1,2] **and Michela Alfè**[1,*]

[1] Institute of Sciences and Technologies for Sustainable Energy and Mobility (CNR-STEMS), National Research Council, Via G. Marconi 4, 80125 Napoli, Italy
[2] Department of Physics 'E. Pancini', University of Naples 'Federico II', Napoli, Italy
[3] Faculty of Mathematics and Physics, Department of Surface and Plasma Science, Charles University, Prague, Czech Republic
[4] Elettra—Sincrotrone Trieste, s.s. 14, km 163.5 34149 Basovizza, Trieste, Italy
[5] CNR-SPIN, Instiute for SuPerconductors, INnovative materials, and devices, Naples, Italy
[*] Authors to whom any correspondence should be addressed.

E-mail: roberto.dicapua@unina.it and michela.alfe@stems.cnr.it

Keywords: MOF, nanostructures, hybrids, graphene-related materials, ssNMR, NEXAFS, XANES

Supplementary material for this article is available online

OPEN ACCESS

RECEIVED
14 May 2024

REVISED
17 July 2024

ACCEPTED FOR PUBLICATION
8 August 2024

PUBLISHED
20 August 2024

Abstract

Hybrids based on the copper-based metal–organic framework HKUST-1 and graphene-like materials (GL) have been synthesized at different concentrations of GL, and investigated by means of solid state nuclear magnetic resonance (ssNMR) and x-ray absorption techniques (NEXAFS and XANES) with the aim of elucidating the effect of the hybridization on the structural properties of HKUST-1. The comparative analysis of ssNMR and x-ray absorption spectra recorded on parent materials (GL and pure HKUST-1) and on the hybrids indicates that the overall structural features of HKUST-1 are preserved in the presence of increasing GL amounts (up to 30 wt.%) and confirms that the framework development is not massively altered by the presence of graphene-related materials (GRMs) in the synthetic medium.

1. Introduction

Metal–organic frameworks (MOFs) are highly porous crystalline materials self-assembled by coordination bonds between metal ions (or metal clusters) and organic linkers with a very broad application array [1]. The integration of MOFs and functional materials as graphene-related materials (GRMs) is gaining an increasing interest [2–7] both in consolidated topics (gas storage and separation [8, 9], catalysis and photocatalytic applications including the degradation of pollutants [10–12], electrochemical applications [13, 14], gas sensing [15]) and in emerging fields (electrochemical sensors [16], energy storage [17, 18], microwave adsorption [19], corrosion resistance [20], and solid-phase microextraction [21]).

Such interest in GRMs as possible carbon-based components in MOF hybrids raises from their unique structure, low toxicity in most cases, and excellent electronic, thermal, electrochemical, and mechanical properties [22]. The presence of heteroatom-containing functional groups and sp^2 aromatic domains enambls GRMs to participate in coordination bonding with metal ions, influencing the growth of MOF crystal leading to structures beneficying the interaction between MOF and GRM [2, 5, 6]. Graphene (G), graphite oxide, graphene oxide (GO), reduced graphene oxide (rGO) and multiwalled carbon nanotubes (MWCNTs) are the most used materials of the wide GRM family. Carbon black, coke, carbonized/pyrolyzed wastes are alternative sources of GRMs both few-layered and multi-layered, as well as bio-precursors and biomasses transformed through many approaches (thermal methods, chemical activation, hydrothermal methods, template-based confinement method and combined approaches) [23–31]. Given this high variability, the quality and the characteristics of the GRMs are highly influenced by the nature of the precursor and the production technique adopted. MOF/GRMs hybrids are promising structures since

synergistic effects between most relevant properties of MOF (such as controlled porosity, selectivity, catalytic activity) and the GRMs properties (such as electric conductivity, broadband light absorption, mechanical stability) [2, 5, 6] can be achieved. The presence of GRMs in MOF-based hybrids allows for: (i) the formation of a conductive bridge for electron transfer; (ii) an improved stability; (iii) structure distortion and modifications; (iv) an enhanced phase dispersion; (v) synergistic effects; (vi) an increased availability of active sites and (vii) larger specific surface areas [2, 5, 6]. The mechanisms involved at the interface between the MOF and GRMs are not completely understood, and the full description and modeling of these systems is still a challenging topic that needs advanced diagnostic techniques. Indeed, if the realization of MOFs composites with GRMs surely enhances the stability of MOFs and some key properties such as electrical conductivity and catalytic activity, it is not obvious how the interaction with GRMs affects the structural properties of MOFs. On this topic, different results have been so far reported, depending on the synthesis method and parameter and on the specific choices of parent MOF and GRM. The preservation of MOF crystal structure or the formation of well-structured nanocomposites have been often reported; conversely, some works report dramatic changes in the MOF structure, and the formation of disordered nanocomposites, the occurrence of structural changes and consequent order-disorder transitions, unregular growth of MOF in carbonaceous sheets triggered by coordination of metal ions with GRM functional groups (see reviews in [6, 32, 33]). Therefore, the observation of macroscopic physicochemical properties cannot be directly associated to microscopic information, and a deeper knowledge of specific realized composites requires to employ appropriate characterization techniques able to achieve structural, electronic, and spectroscopical information.

Solid state nuclear magnetic resonance (ssNMR) is a valuable spectroscopic technique for MOF characterization and can be considered as complementary to x-ray dif-fraction (XRD) methods [34–36]. ssNMR allows for identifying structural parameters (including distance measurements) as well as detecting dynamical effects, thanks to its high sensitivity to local structure around the nucleus of interest, without any requirement for longer-range order [34–36]. ^{1}H and ^{13}C magic-angle spinning (MAS) NMR experiments on MOF are mainly used to confirm the incorporation of organic linkers and to verify their functionalities and their local order when involved in the framework, to follow dehydration/desolvation processes and to monitor the adsorption of organic guest species [34–37]. Moreover, ssNMR experiments allow for collecting information on host–guest interactions determining the flexibility as well as adsorption-induced structural changes of the host, the mobility of the host lattice as well as the mobility of the adsorbed species [35–37]. For example, ssNMR has been employed for studying the interactions of HKUST-1 with water [38], ammonia [39], CO and CO_2 [40], and NO [41].

On MOFs, x-ray absorption techniques have been mainly employed to probe the oxidation state of metal ions (Cu or Ni, for example), in order to investigate some specific properties such as the features of metal defective site, the effects of thermal treatments or x-ray exposure, the role of chemical species in catalytic activity [42–44].

Near-edge x-ray absorption fine structure (NEXAFS) and x-ray absorption near edge structure (XANES) spectroscopies probe electronic transitions from the deepest core-shell (the K-edge) of an atomic species involved in molecular orbitals to intra-molecular and extra-molecular higher-energy states. The excitation of core electrons into unoccupied or continuum states causes the absorption of incident x-rays, which can be measured as a function of the energy of the incident photon. The analysis of distinctive features in the adsorption spectra (typically up to 50 eV above the K-edge), and of their differences in the comparison of different samples, makes NEXAFS and XANES powerful structural tools providing information on the electronic structure and on the chemical environment of the absorber species [45].

Few reports are present about ssNMR and x-ray absorption measurements on MOF-based hybrid materials. In such cases, NEXAFS measurements are mainly devoted to the characterization of valence states or conduction bands associated to metallic species [44, 46]. Jagódka *et al* try to investigate the influence of the type of GRM and synthesis parameters on the physicochemical properties of HKUST-1/GO and HKUST-1/rGO by standard characterization techniques (x-ray diffraction, scanning and transmission electron microscopy, Fourier transform infrared spectroscopy, thermogravimetric analysis) and x-ray photoelectron spectroscopy [47].

In this paper, graphene-like materials (GL), short stacked graphenic layers with lateral dimensions around 50 nm [48] obtained through a chemical destructuration of a nanostructured carbon black [49] have been selected as GRM, being water-stable and thus compatible with the synthesis via wet chemistry. The GL and its characteristics were widely described elsewhere [48–57]. The GL small dimensions and the presence of oxygen functional groups (mainly carboxylic and carbonyl groups located at the edges of the graphenic layers [50, 51]) limit aggregation phenomena allowing high colloidal stability in a wide pH range, from 3 to 14, without the use of any surfactant [50]. The capacity to produce stable water suspensions makes GL good

candidates for the production of hybrid materials through wet chemical approaches [7, 52–54] and processing by sophisticated deposition techniques (inkjet printing and MAPLE) [55, 56]. The presence of intact graphenic basal planes within GL materials ensures good thermal, optical and electrical conductive properties [49, 50, 57]. GL materials exhibit also low toxicity towards eukaryotic cells [56], antimicrobial activity [58] and a proven biocompatibility on a vertebrate model [48].

HKUST-1, despite the difficulties of the investigation via ssNMR, related to the paramagnetic nature of copper ions, has been selected as MOF structure because it is one of the most studied MOFs and thus because it represents a benchmark.

In this work, ssNMR was applied comparatively to x-ray absorption techniques to investigate HKUST-1, GL and three hybrids obtained by combining GL and HKUST-1. Two hybrid materials were obtained allowing the growth of the HKUST-1 framework in the presence of 15% and 30% GL amounts. The GL wt. percentages of the investigated hybrid compounds were chosen according to our study on dc electrical conductivity on these materials [7], as the ones which determined a detectable electrical conductivity compared to the insulating HKUST-1 parent compound, but still much lower (6–7 orders of magnitude) than pure GL, and before the steep increase of such conductivity value close to the pure GL one for slightly higher percentage of GL inclusion. Also, for these hybrid compositions we measured a pore volume still not smaller then 2/3 of the 'original' pore volume of the pure HKUST-1, while already at 40% GL the pore volume was less than half of that of HKUST-1 [7] (making the hybrids with higher GL amount less interesting for many applications).

2. Materials and methods

All chemicals were purchased from Sigma-Aldrich S.r.l. (ACS grade) and used without further purification. Carbon black (CB, furnace black, N110 type, 15–20 nm primary particles diameter) was kindly provided by Sid Richardson Carbon Co.

2.1. Samples synthesis

GL were obtained applying a two-step synthetic strategy described in previous works [49, 50]. The synthetic procedure is reported in the supporting information section.

Cu-HKUST-1 was produced applying the synthetic approach reported in [8] and reported in the supporting information. The hybrid materials named HKUST-1/GL-15, and HKUST-1/GL-30 (where 15 and 30 stand for the theoretical GL percentage incorporated, that is 15 and 30 wt.%, respectively) were prepared in accordance with the synthetic approach reported in [7, 8]. To prepare hybrid materials containing growing amounts of incorporated GL, the following amounts of GL as water suspension (2.5 mg ml^{-1} as mass concentration) were mixed with the DMF/ethanol mixture already containing 1 g of $Cu(NO_3)_2 \cdot 2.5\ H_2O$, 0.5 g of BTC: 105 mg and 210 mg of GL for the preparation of HKUST-1/GL-15 and HKUST-1/GL-30, respectively.

2.2. Methods

ssNMR measurements were performed at the Slovenian NMR Center in Ljubljana Varian 600 MHz VNMRS spectrometer equipped with a 3.2 mm HX MAS probe was used for the acquisition of ^{1}H and ^{13}C MAS, and ^{1}H–^{13}C cross-polarization magic-angle spinning spectra. The instrument was operated under the experimental parameters reported in [53] and briefly reported in the supporting information section. XANES experiments were carried out at the XAFS beamline at Elettra Synchrotron (Basovizza, Trieste, Italy) [59]. Copper K-edge absorption spectra on HKUST-1, GL materials, and HKUST-1/GL hybrid materials, as well as on CuO and Cu_2O used as reference, were collected in the energy range from 8780 eV to 10 000 eV with an energy step size of 0.2 eV around the absorption edge, in transmission mode with a standard ionization chambers for the detection of intensities, using Si(111) monochromator calibrated to the first-derivative maximum of the K-edge absorption spectrum of a metallic Cu foil (8979 eV). The samples were prepared by gentle pressing the powders between Kapton® tape.

X-ray photoemission spectroscopy (XPS) and NEXAFS measurements were performed at the materials science beamline, Elettra synchrotron (Basovizza, Trieste, Italy), in an ultra-high vacuum chamber with a base pressure of 2×10^{-10} mbar. For XPS, the chamber was equipped with a dual Mg/Al x-ray source and a Súpecs Phoibos 150 hemispherical energy analyzer. Al Ka radiation (1486.6 eV) was used to measure the core levels of C 1*s* and Cu 2*p*, with total resolutions of 1 eV for both acquisitions. NEXAFS measurements were performed in the Auger-electron yield mode near the C-edge at less than 0.4 eV resolution.

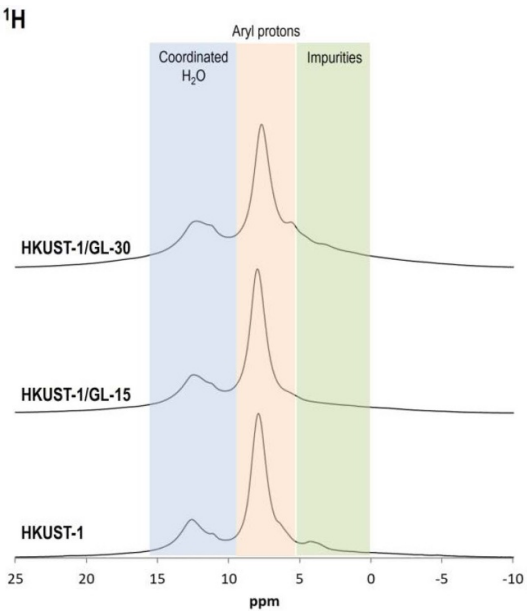

Figure 1. ^{1}H-NMR spectra of HKUST-1/GL-15 and HKUST-1/GL-30. The spectrum of HKUST-1 is also reported for comparison.

3. Results and discussion

The morphology, crystallinity, and thermal stability were checked for the parent material HKUST-1 and the hybrids. The obtained results were in line with those of previous preparations [7, 8]. The reliability and reproducibility of the synthesis method as well as the study on how much GL was included into the HKUST-1 structure was addressed in [7, 8], finding that a complete incorporation of the carbonaceous layers into the hybrids was obtained, without significant loss of materials. For the sake of completeness, these results are reported as supporting information material.

In figure 1, the ^{1}H MAS spectra of HKUST-1 and of the hybrids are contrasted. The spectra are normalized to the maximum height and vertically shifted for clarity.

The central peak of the HKUST-1 ^{1}H MAS spectrum at 7.93 ppm is ascribable to the ring protons of the linker (BTC), while the peak around 12 ppm is due to adsorbed water; the presence of adsorbed water causes a shift of the signal of BTC protons to lower chemical shifts compared to the value reported by other authors [39, 40]. The features of ^{1}H MAS spectra on HKUST-1 are essentially preserved in HKUST-1/GL-15 and HKUST-1/GL-30 spectra (with only a slightly lower chemical shift on HKUST-1/GL-30). The similarity of these spectra indicates a similar chemical and electronic environment for hydrogen atoms in the pristine MOF and in the hybrids. This result is consistent with the fact that XRD measurements (reported in the supplemental materials) reveal that the framework structure is unperturbed by the inclusion of GL.

In figure 2, the ^{13}C MAS spectrum of HKUST-1 and those of the hybrids are contrasted. The spectrum of GL is reported for comparison. Spectra have been vertically shifted for clarity. The signals in the ^{13}C MAS spectrum of HKUST-1 have been assigned in accordance with the work of Dawson *et al* [38] as follows: the signal at −80.9 ppm was assigned to the carboxylate (CO_2^-) group of the linker coordinated to the metal center (Cu^{2+}), the sharp signal at 229.7 ppm to the aromatic carbons bearing a H (C=CH), the broad signal around 800 ppm to quaternary carbons within the aromatic ring of the linker. The other small signals in the spectrum were classified as sidebands or impurities belonging to the synthetic medium.

The ^{13}C MAS spectra of the hybrids exhibit the same peaks of HKUST-1, but with the increase of GL loading the intensity of the peaks overlapping between 80–180 ppm ascribable to the graphitic network of GL [53] also increases. A little shift of the peaks ascribable to the framework components in the spectra of the hybrid compared to that of HKUST-1 was sometimes detected and related to the presence of adsorbed water molecules. In accordance with [40], water adsorption has a strong effect on the carboxylate carbon resonance, which is shifted to a higher frequency because water coordinated to copper changes the coordination geometry from square-planar to square pyramidal, which affects the electronic configuration of copper [40].

C K-edge NEXAFS spectra recorded on all the investigated samples are reported in figure 3. Spectra have been vertically shifted for clarity. The peak resonances in the absorption pre-edge spectral region (photon energies below the ionization step) on HKUST-1 and hybrids exhibit quite different structures. At the lowest

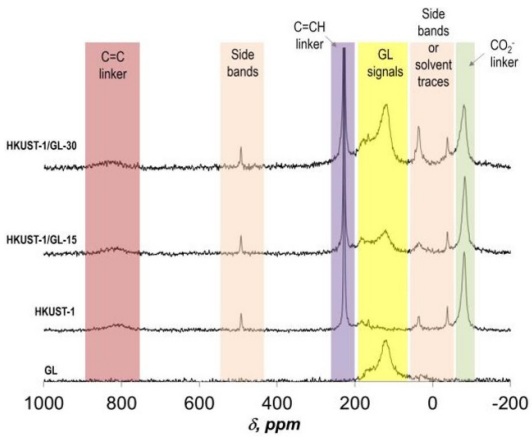

Figure 2. ^{13}C-NMR spectra of HKUST-1/GL-15 and HKUST-1/GL-30. Spectra of HKUST-1 and GL are also reported for comparison.

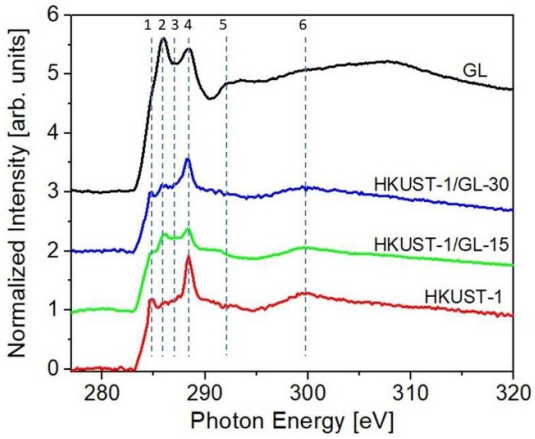

Figure 3. Comparison among the C K-edge NEXAFS spectra recorded on HKUST-1/GL-15 and HKUST-1/GL-30. The spectra of HKUST-1 and GL are also reported for comparison; some spectral features are highlighted and numbered accordingly with the description in the main text.

energy side, the NEXAFS spectrum of HKUST-1 shows a sharp resonance at 284.8 eV (identified as peak 1 in figure 3) and a second very sharp peak at 288.4 eV (peak 4). The latter constitutes the dominant feature in the spectrum (as well as in the spectra of hybrid materials).

In the NEXAFS spectrum of the GL, this second resonance is preserved, even if the correspondent peak is much more broadened than in HKUST-1, and it is no longer the highest peak. On the contrary, the lowest energy peak at 284.8 eV is still present but as a shoulder of a more intense peak located at higher energy, 286.0 eV (named peak 2); as for peak 4, also peak 2 is characterized by a width larger than the spectral maxima recorded on HKUST-1. A spectral feature corresponding to peak 2 can also be observed in the NEXAFS spectrum of HKUST-1, but here it is much less intense and defined, included between the two main peaks together with some other minor spectral structures between 286.6 eV and 287.4 eV.

Both peak 1 at 284.8 eV and peak 2 at 286.0 eV originate from C1*s* $\rightarrow \pi^*$ transitions, electronic excitations of carbon 1*s* core electrons to the first unoccupied anti-bonding molecular orbital. In particular, peak 1 can be ascribed to C=C C1*s* $\rightarrow \pi^*$ transitions [60–64]. In this respect, its larger broadening in GL spectrum, where it appears as a shoulder and seems to extend to higher energies, partially covered by peak 2, is an effect of the higher structural disorder in GL than in the MOF; in addition, for graphitic and graphenic sp^2 carbon, such transition is often reported at energies around 285 eV or slightly higher, therefore making expectable the observed width of this spectral feature in GL spectrum [61–64]. Peak 2 could be assigned to C=C, C=O, C=N 1*s* $\rightarrow \pi^*$ or C–O 1*s* $\rightarrow \sigma^*$ excitations [60, 62, 63, 65]; its intense and broad character in GL NEXAFS spectrum is likely a signature of the contribution of the different functional groups characterizing the surface of this material [50, 51]. It can be considered a fingerprint of the GL character compared to HKUST-1. The occurrence of C=O C1*s* $\rightarrow \pi^*$ transitions is however confirmed by the presence of peak 4 at 288.4 eV [60, 61, 63] on both parent materials. Despite both GL and HKUST-1 (and also the two

hybrids) show peak 4 as a strong resonance, it is interesting to remark some differences: first, the already mentioned broadening of this feature in GL compared to HKUST-1; second, the presence of a very broad feature around 300 eV (peak 6) in HKUST-1, much less pronounced in GL, that can be assigned to the corresponding C=O C1*s* $\rightarrow \sigma^*$ excitation [61, 63]. These remarks suggest that the origin of the common feature marked as peak 4 could be different in the two pristine compounds; it is likely due mainly to carboxylic functional groups in GL, while in HKUST-1, it could have risen from the carbon–oxygen bonds in the structure. The presence of a fine structure between peak 1 and peak 4 in HKUST-1 was also highlighted. One of the peaks belonging to such interval is the already discussed peak 2; the other modulations of the NEXAFS spectrum in this energy interval could be ascribed to C–H, C–O, C–O–C 1*s* $\rightarrow \sigma^*$ electronic excitations [60, 63, 65]. We assign to C–H 1*s* $\rightarrow \sigma^*$ transitions the feature named peak 3, which is present in GL (the only distinguishable on this sample in the energy interval between the main peaks) around 287 eV, but not in HKUST-1 and hybrid materials, constituting another remarkable difference. It represents a transition of 1*s* core electrons towards valence/Rydberg states (C–H* from aromatic/alkyl C–H) [60, 63].

A weak shoulder-like signature slightly above 290 eV can be observed in HKUST-1 NEXAFS spectrum; such a shoulder has already been observed in C1*s* NEXAFS spectra of CuO/graphene and of Cu-, Fe-, Cr-MWCNT hybrids [65–68]. It is interesting to note that the addition of Cu to MWCNT in [37] actually enhanced the spectral features around 287 eV in the NEXAFS spectrum, and also provoked the displacement of spectral weight from the 285 eV band to the 288 eV one: both occurrences have been observed in our Cu-based HKUST-1 NEXAFS spectrum.

Finally, we remark on the presence of an additional spectral feature, peak 5, much more pronounced in the GL spectrum than in HKUST-1 one, at about 292 eV (shifted to higher energies in HKUST-1 spectrum), due to excitations of C=C 1*s* $\rightarrow \sigma^*$ [61, 63].

After the detailed description of the main spectral features detectable on the pristine compounds, more insights about the effect of GL inclusion into MOF structure can be inferred by analyzing the C NEXAFS spectra of hybrid materials.

The two most remarkable peak resonances on the HKUST-1 spectrum exhibit a clear evolution when the amount of GL increases. In HKUST-1/GL-15 and HKUST-1/GL-30, containing 15 wt.% and 30 wt.% respectively, peak 1 and peak 4 lose spectral weight, approaching that in the pure GL spectrum. Peak 2 also follows a similar evolution: in HKUST-1 it has an intensity lower than peak 1 and peak 4; conversely, in HKUST-1/GL-15 and HKUST-1/GL-30 it appears higher than peak 1, evolving towards the condition of GL spectrum where peak 1 is almost entirely hidden by peak 2. It is worth noting that a comparison between the intensity of peaks 1 and 4 can still be made among the NEXAFS spectra of the hybrids, exactly because the first one has not yet been covered by peak 2. A fast estimation shows that the height ratio between peaks 1 and 4, while both lose weight in the spectrum, is roughly preserved when the GL percentage increases. This circumstance suggests that the GL inclusion is not detrimental for the HKUST-1 structural and chemical features (NEXAFS resonances are sensitive to the chemical environment of the absorbing atoms).

As concerns the other spectral signatures, they follow a general trend of evolution from HKUST-1 to GL character, but some differences can be remarked, indicating a different role of the associated electronic, structural, and spectroscopic properties. Peak 3, for instance, although less evident among those peculiar of GL with respect to HKUST-1, arises in the spectra of hybrid materials; at the same time, the Cu-related spectral features at similar energies disappear. On the contrary, a 'jump' identified as peak 5, strongly marked in the GL spectrum, does not look to show up in the spectra of hybrids even at the highest employed GL concentration. Peak 3 is associated to transitions to nearly continuous allowed energies, namely Rydberg states; as a consequence, we can speculate that such circumstance indicates that, while discrete levels or orbitals coming from pristine compounds are essentially preserved in the hybrids, valence states are affected by the interaction with the surrounding HKUST-1 matrix. In such a frame, the mixing of valence state characters could play a role in triggering the percolation mechanism that we revealed in [7] as underlaying at the base of the conducting behavior of HKUST-1/GL hybrids. The disappearance of Cu-related HKUST-1 spectral features can be due to the same rearrangement of valence electrons.

Differently from the rich variety of the C K-edge NEXAFS spectra acquired on the different samples, the Cu K-edge XANES spectra are extremely similar for HKUST-1 and the two hybrid materials (figure 4, panel (a)). This is not surprising: While the C features are related to the several bonds and functional groups which are intrinsically different in the pure materials (HKUST-1 and GL), the Cu spectral features are mainly driven by the Cu state in HKUST-1. The strong similarity between the Cu K-edge XANES data of HKUST-1 and hybrids indicates that such general spectral features remain essentially unchanged by the inclusion of carbonaceous component in the hybrids up to 30 wt.%.

To go in deeper detail, the only remarkable evolving feature in the Cu K-edge XANES spectra is constituted by the pre-peak slightly below 8985 eV, which becomes less sharp in the spectra of hybrid materials with the largest content of GL. This is a spectral feature ascribable to the presence of Cu(II), while

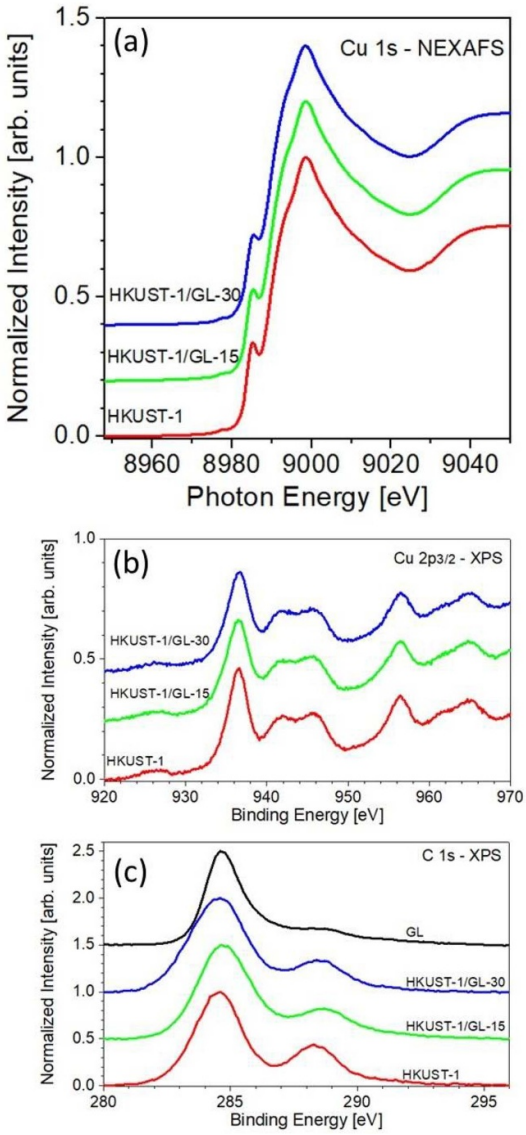

Figure 4. (a) comparison among the Cu K-edge XANES spectra recorded on HKUST-1 and hybrid samples; (b) comparison among the Cu 2*p* XPS spectra recorded on HKUST-1 and hybrid samples; (c) comparison among the C 1*s* XPS spectra recorded on all the investigated samples. All the spectra in the plots have been vertically shifted for clarity.

the distinctive feature of Cu(I), expected at a lower energy, is basically missing in all the samples. The fact that Cu(II) is the largely dominant oxidation state in our samples is confirmed by the comparison with reference CuO (Cu(II)) and Cu_2O (Cu(I)) XANES spectra reported in the supplementary information. In addition, there is no evidence of spectral features associated to Cu in the metallic state [69, 70]. The absence of metallic Cu is in agreement with the electrical insulating character of HKUST-1, and it confirms that the electrical conductivity arising in the HKUST-1/GL hybrids is not related to modifications in the copper electronic state.

XPS spectra have been acquired at Cu 2*p* and C 1*s* core levels and reported in figures 4(b) and (c). They confirm the general trend observed by NEXAFS and XANES measurements, i.e. a substantial similarity among the Cu XPS spectra (on HKUST-1 and hybrids) and, conversely, a wider variability for the C XPS spectral feature (recorded on all the materials). In particular, in the C 1*s* spectrum of GL, the pronounced broadening of the spectral feature around 288–289 eV, resulting from the overlapping of contributions from C atoms involved in several functional groups, is a further indication of the greater disorder in surface chemistry of GL materials.

4. Conclusions

Solid State—Nuclear Magnetic Resonances and x-ray absorption spectroscopic measurements (NEXAFS and XANES) provided structural and spectroscopic information on the inclusion of GL into the HKUST-1 structure. Interestingly, ^{1}H MAS and ^{13}C MAS NMR spectra indicated that also the hybrids HKUST-1/GL-15

and HKUST-1/GL-30 exhibit structural features similar to the parent HKUST-1. From the spectroscopic point of view, it is remarkable that NEXAFS spectra on HKUST-1/GL-15 and HKUST-1/GL-30 do not exhibit any signature of the strong broadening of absorption peaks which are a key feature of the more disordered structure of GL. This indicates that the GL units are embedded in the ordered framework of HKUST-1 as revealed by XRD rather than being dispersed in it with somehow distributed allocations and orientations. Also, in the hybrids we observed a dramatic decrease of the spectral weight of peaks associated to functional groups from GL (peak 2) and to Rydberg states (from aromatic/alkyl C–H): it represents a further indication of the inclusion of GL inside the hybrid structure, since from a mere physically hybrid mixture we would likely expect a strong signature of these original features coming from the pure GL chemistry (for the difference with a mere physical mixture, TGA and porosity results reported in [7] are also relevant). As a confirmation of the above consideration, the TGA curves in oxidative environments (Supplementary Information) of a physical mixture of the two components of HKUST-1/GL-15 built mixing at the appropriate % wt. the two pure components (GL and HKUST-1), presents a distinct weight drop around 500 °C attributed to the combustion of the GRM component. The absence of such drop in the TGA plot of the corresponding hybrid (figure S1) indicates a good inclusion of the graphenic component into the hybrid.

It also means that the gradual deterioration of surface morphology when increasing GL amount, as shown by SEM images (supplementary information), must be ascribed to a supramolecular more disordered arrangement rather than a crystalline disorder. In the Supplemental Information we added a sketch of the structural model suggested by our measurements. Such inclusion, as well as the evidence of the mixing of valence characters of the pristine materials, likely plays a key role in the percolating mechanism at the base of the electrical conductivity enhancement with the GL amount, that in a previous work [7] we demonstrated being the main responsible of the enhancement of dc electrical conductivity of HKUST-1/GL hybrids compared to the pristine HKUST-1.

Data availability statement

All data that support the findings of this study are included within the article (and any supplementary files).

Acknowledgments

The authors acknowledge the CERIC-ERIC Consortium for the financial support and access to experimental facilities at materials science beamline (MSB), Elettra Synchrotron in Trieste and at the Slovenian NMR Center of Ljubljana under proposal 20142026. VG and MA acknowledge the networking support by the COST Action CA19118 EsSENce, supported by the COST Association (European Cooperation in Science and Technology). C.C. acknowledges the Project 'EMBRC UP'—EMBRC Unlocking the Potential for health and food from the seas, CUP: C63C22000570001—Project code IR0000035 for PhD fellowship founding.

All the authors wish to remember and honor the memory of Gregor Mali, who passed away prematurely before the completion of this manuscript, and whose scientific and human contribution was decisive for the realization of the work described in it.

Author contributions

Valentina Gargiulo Conceptualization, Methodology, Investigation, Validation, Data Curation, Visualization, Funding acquisition, Project administration, Writing—Original Draft, Writing—Review & Editing; **Roberto Di Capua** Conceptualization, Methodology, Investigation, Validation, Formal analysis, Resources, Funding acquisition, Supervision, Writing—Original Draft, Writing—Review & Editing; **Giuliana Aquilanti, Tomáš Skála, Michael Vorochta** Methodology, Investigation, Validation, Supervision, Writing—Review & Editing; **Claudio Clemente** Data Curation, Visualization, Writing—Review & Editing **Michela Alfe** Conceptualization, Methodology, Investigation, Validation, Resources, Supervision, Writing—Review & Editing.

Conflict of interest

The authors declare no competing financial interest.

ORCID iDs

Valentina Gargiulo https://orcid.org/0000-0002-6517-2263
Roberto Di Capua https://orcid.org/0000-0003-3605-0993
Michael Vorochta https://orcid.org/0000-0001-8382-7027
Giuliana Aquilanti https://orcid.org/0000-0001-6683-2668
Tomáš Skála https://orcid.org/0000-0003-2909-9422
Michela Alfè https://orcid.org/0000-0001-8930-1210

References

[1] Safaei M, Foroughi M M, Ebrahimpoor N, Jahani S, Omidi A and Khatami M 2019 *Trends Anal. Chem.* **118** 401–25
[2] Zheng Y, Zheng S, Xue H and Pang H 2018 *Adv. Funct. Mater.* **28** 1804950
[3] Zhang Q, Yang H, Zhou T, Chen X, Li W and Pang H 2022 *Adv. Sci.* **9** 2204141
[4] Xue Y, Zheng S, Xue H and Pang H 2019 *J. Mater. Chem.* A **7** 7301
[5] Muschi M and Serre C 2019 *Coord. Chem. Rev.* **387** 262–72
[6] Jayaramulu K *et al* 2022 *Chem. Rev.* **122** 17241–338
[7] Alfè M, Gargiulo V, Lisi L and Di Capua R 2014 *Mater. Chem. Phys.* **147** 744–50
[8] Alfè M, Policicchio A, Lisi L and Gargiulo V 2021 *Renew. Sustain. Energy Rev.* **141** 110816
[9] Gargiulo V, Policicchio A, Lisi L and Alfe M 2023 *Energy Fuels* **37** 5291–302
[10] Thi Q V, Tamboli M S, Ta Q T H, Kolekar G B and Sohna D 2020 *Mater. Sci. Eng.* B **261** 114678
[11] Olowoyo J O, Saini U, Kumar M, Valdes H, Singh H, Omorogie M O, Babalola J O, Vorontsov A V, Kumar U and Smirniotis P G 2020 *J. CO_2 Util.* **42** 101300
[12] Wu S-C, Yu -L-L, Xiao -F-F, You X, Yang C and Cheng J-H 2017 *J. Alloys Compd.* **724** 625–32
[13] Zuo K *et al* 2020 *Environ. Sci. Technol.* **54** 13322–32
[14] Qiu Z, Li Y, Gao Y, Meng Z, Sun Y, Bai Y, Suen N-T, Chen H-C, Pi Y and Pang H 2023 *Angew. Chem., Int. Ed.* **62** e202306881
[15] Gargiulo V, Alfè M, Giordano L and Lettieri S 2020 *Chemosensors* **10** 290
[16] Golsheikh A M, Yeap G-Y, Yam F K and Lim H S 2020 *Synth. Met.* **260** 116272
[17] Peng Y, Xu J, Xu J, Ma J, Bai Y, Cao S, Zhang S and Pang H 2022 *Adv. Colloid Interface Sci.* **307** 102732
[18] Zhang M, Shan Y, Kong Q and Pang H 2022 *FlatChem* **32** 100332
[19] Bai Y-W, Shi G, Gao J and Shi F-N 2021 *J. Phys. Chem. Solid.* **148** 109657
[20] Wei W, Liu Z, Wei R, Han G-C and Liang C 2020 *RSC Adv.* **10** 29923–34
[21] Liu H, Fan H, Dang S, Li M, Gu A and Yu H 2020 *Chromatographia* **83** 1065–73
[22] Tiwari S K, Sahoo S, Wang N and Huczko A 2020 *J. Sci.: Adv. Mater. Devices* **5** 10–29
[23] Saha S, Lakhe P, Mason M J, Coleman B J, Arole K, Zhao X, Yakovlev S, Uppili S, Green M J and Hule R A 2021 *2D Mater. Appl.* **5** 75
[24] Sierra U, Álvarez P, Blanco C, Granda M, Santamaria R and Menendez R 2015 *Carbon* **93** 812–8
[25] Sierra U, Álvarez P, Blanco C, Granda M, Santamaría R and Menéndez R 2016 *Fuel* **166** 400–3
[26] Sierra U, Mercado A, Cuara E, Barriga-Castro E D and Cortés A 2020 *Fuel* **262** 116455
[27] Vieira O, Ribeiro R S, Diaz de Tuesta J L, Gomes H T and Silva A M T 2022 *Chem. Eng. J.* **428** 131399
[28] Kong X *et al* 2020 *Chem. Eng. J.* **399** 125808
[29] Raghavan N, Thangavel S and Venugopal G 2017 *Appl. Mater. Today* **7** 246–54
[30] Poorna A R, Saravanathamizhan R and Balasubramanian N 2021 *Electrochem. Sci. Adv.* **1** e2000028
[31] Safian M T U, Haron U S and Ibrahim M M 2020 *BioResources* **15** 9756
[32] Shinde S K, Kim D-Y, Kumar M, Murugadoss G, Ramesh S, Tamboli A M and Yadav H M 2022 *Polymers* **14** 511
[33] Nazir M A, Javed M S, Islam M, Assiri M A, Hassan A M, Jamshaid M, Najam T, Shah S S A and Ur Rehman A 2024 *Compos. Commun.* **45** 101783
[34] Sutrisno A and Huang Y 2013 *Solid State Nucl. Magn. Reson.* **49–50** 1–11
[35] Hoffmann H C, Debowski M, Müller P, Paasch S, Senkovska I, Kaskel S and Brunner E 2012 *Materials* **5** 2537–72
[36] He C, Li S, Xiao Y, Xu J and Deng F 2022 *Solid State Nucl. Mag.* **117** 101772
[37] Xiao Y, Li S, Xu J and Deng F 2022 *Curr. Opin. Colloid Interface Sci.* **61** 101633
[38] Dawson D M, Jamieson L E, Infas M, Mohideen H, McKinlay A C, Smellie I A, Cadou R, Keddie N S, Morris R E and Ashbrook S E 2013 *Phys. Chem. Chem. Phys.* **15** 919
[39] Peterson G W, Wagner G W, Balboa A, Mahle J, Sewell T and Karwacki C J 2009 *J. Phys. Chem.* C **113** 13906–17
[40] Gul-E-Noor F, Jee B, Pöppl A, Hartmann M, Himsl D and Bertmer M 2011 *Phys. Chem. Chem. Phys.* **13** 7783–8
[41] Khan A H, Peikert K, Fröba M and Bertmer M 2015 *Micropor. Mesopor. Mater.* **216** 111–7
[42] Braglia L, Tavani F, Mauri S, Edla R, Krizmancic D, Tofoni A, Colombo V, D'Angelo P and Torelli P 2021 *J. Phys. Chem. Lett.* **12** 9182–7
[43] Nijem N, Bluhm H, Ng M L, Kunz M, Leone S R and Gilles M K 2014 *Chem. Commun.* **50** 10144
[44] Zhao S *et al* 2020 *Nat. Energy* **5** 1–10
[45] Hahner G 2006 *Chem. Soc. Rev.* **35** 1244–55
[46] Chen Y, Sakata O, Nanba Y, Kumara L S R, Yang A, Song C, Koyama M, Li G, Kobayashi H and Kitagawa H 2018 *Commun. Chem.* **1** 61
[47] Jagódka P, Matus K and Łamacz A 2022 *Molecules* **27** 7082
[48] d'Amora M, Alfe M, Gargiulo V and Giordani S 2020 *Nanomaterials* **10** 1472
[49] Alfè M, Gargiulo V, Di Capua R, Chiarella F, Rouzaud J N, Vergara A and Ciajolo A 2012 *ACS Appl. Mater. Interfaces* **4** 4491–8
[50] Alfè M, Gargiulo V and Di Capua R 2015 *Appl. Surf. Sci.* **353** 628–35
[51] Gargiulo V, Alfano B, Di Capua R, Alfé M, Vorokhta M, Polichetti T, Massera E, Miglietta M L, Schiattarella C and Di Francia G 2018 *J. Appl. Phys.* **123** 024503
[52] Gargiulo V, Alfè M, Di Capua R, Togna A R, Cammisotto V, Fiorito S, Musto A, Navarra A, Parisi S and Pezzella A 2015 *J. Mater. Chem.* B **3** 5070–9
[53] Di Capua R, Gargiulo V, Alfè M, De Luca G M, Skala T, Mali G and Pezzella A 2019 *Front. Chem.* **7** 121

[54] Amantea F et al 2023 Appl. Surf. Sci. 633 157608
[55] Villani F, Loffredo F, Alfano B, Miglietta M L, Verdoliva L, Alfè M, Gargiulo V and Polichetti T 2019 Graphene-like based-chemiresistors inkjet-printed onto paper substrate Sensors CNS 2018 (Lecture Notes in Electrical Engineering) vol 539, ed B Andò et al (Springer)
[56] Alfe M, Minopoli G, Tartaglia M, Gargiulo V, Caruso U, Pepe G P and Ausanio G 2022 Nanomaterials 12 3663
[57] Ferraiuolo R, Alfe M, Gargiulo V, Pepe G P, Tafuri F, Pezzella A, Ausanio G and Montemurro D 2022 Coatings 12 1788
[58] Olivi M, Alfè M, Gargiulo V, Valle F, Mura F, Di Giosia M, Rapino S, Palleschi C, Uccelletti D and Fiorito S 2016 J. Nanopart. Res. 18 358
[59] Di Cicco A, Aquilanti G, Minicucci M, Principi E, Novello N, Cognigni A and Olivi L 2009 J. Phys.: Conf. Ser. 190 012043
[60] Heymann K, Lehmann J, Solomon D, Schmidt M W I and Regier T 2011 Org. Geochem. 42 1055
[61] Chunjaemsri T, Chanlek N, Sukkha U, Nakajima H, Rujirawat S, Yimnirun R and Kidkhunthod P 2020 Radiat. Phys. Chem. 175 108271
[62] Ehlert C, Unger W E S and Saalfrank P 2014 Phys. Chem. Chem. Phys. 16 14083
[63] Latham K G, Simone M I, Dose W M, Allen J A and Donne S W 2017 Carbon 114 566
[64] Ehlert C, Holzweber M, Lippitz A, Unger W E S and Saalfrank P 2016 Phys. Chem. Chem. Phys. 18 8654
[65] Sivkov D V, Petrova O V, Nekipelov S V, Vinogradov A S, Skandakov R N, Bakina K A, Isaenko S I, Obedkov A M, Kaverin B S and Sivkov V N 2021 Appl. Sci. 11 11646
[66] Sivkov D et al 2020 Nanomaterials 10 374
[67] Sivkov D et al 2020 Appl. Sci. 10 4736
[68] Zhang X, Zhou J, Song H, Chen X, Fedoseeva Y V, Okotrub A V and Bulusheva L G 2014 ACS Appl. Mater. Interfaces 6 17236–44
[69] Gaur A, Shrivastava B D and Joshi S K 2009 J. Phys.: Conf. Ser. 190 012084
[70] Larsson M, Lindén J B, Kaur S, Le Cerf B and Kempson I 2017 Powder Diffr. 32 S28–32